J Mater Sci (2008) 43:5591–5598
DOI 10.1007/s10853-008-2795-7

Effect of oxygen partial pressure on the oxidation behaviour of an yttria dispersion strengthened NiCr-base alloy

E. Essuman · G. H. Meier · J. Zurek · M. Hänsel · L. Singheiser · T. Norby · W. J. Quadakkers

Received: 14 April 2008 / Accepted: 9 June 2008 / Published online: 8 July 2008

Abstract An yttria dispersion strengthened NiCr-base alloy was studied with respect to isothermal oxidation behaviour at 1000 °C and 1050 °C in high- and low-pO_2 gases, i.e. Ar–O_2 and Ar(−H_2)–H_2O. The scale growth kinetics, morphology and composition were studied by thermogravimetry in combination with SEM/EDX and SNMS. Due to Y doping the surface scale is very protective and initially grows predominantly by inward oxygen diffusion. Local formation of mainly outwardly growing oxide nodules occurs after longer oxidation times and is related to metallic protrusions formed as a result of internal oxidation of the minor alloying addition aluminium. The differences in scale morphology in the various environments are related to the effect of the gas composition on scale grain size and on the relative amounts of inward scale growth. Possibly the pO_2 dependence of the Ti-solubility in the chromia scale and/or hydrogen doping of the oxide plays an additional role in the scale growth process.

Introduction

NiCr—base alloys are commercially used construction materials for a large number of high temperature components. For protection against oxidation attack the materials rely on chromia base scales which form on the component surfaces during high temperature service due to selective oxidation of the alloying element chromium. Frequently, the NiCr—base materials are alloyed with one or more elements to increase their creep resistance by solid solution and/or precipitation strengthening. The most commonly used precipitates to obtain an increase in the creep resistance of Ni-base alloys are carbides and phases based on γ'-Ni_3Al. The strengthening imparted by this mechanism is rapidly lost at high service temperatures of about 900 °C due to precipitation dissolution and/or coarsening [1–3]. These effects can largely be suppressed if dispersions of a thermodynamically stable oxide are used for strengthening. A number of NiCr-base alloys, which contain dispersions of a stable oxide, mainly yttria, have been developed by several alloy manufacturers. Typical dispersions of particles of 10 nm diameter and approximately 30 nm apart can be obtained by a special milling process called Mechanical Alloying [4, 5]. The use of yttria has the additional advantage that precipitates of this oxide greatly improve the oxidation resistance in a similar manner to that obtained by metallic additions of yttrium or other so-called reactive elements (REs); it decreases the growth rate and improves the adherence of the chromia base oxide scale [6–8]. The oxidation behaviour of NiCr-base ODS alloys has been described in a number of publications (e.g. [6, 9, 10]). However, practically all these studies are related to the materials behaviour in air, oxygen or inert gas/oxygen mixtures. As far as known to the authors, few studies exist on the behaviour of the materials mentioned in low-pO_2 gases in which water vapour is the main oxygen carrying species. Knowledge about the behaviour in this type of environment is of great importance because chromia forming alloys are frequently used in low-pO_2 gases and a

E. Essuman · J. Zurek (✉) · M. Hänsel · L. Singheiser · W. J. Quadakkers
Forschungszentrum Jülich, IEF-2, 52428 Julich, Germany
e-mail: j.zurek@fz-juelich.de

E. Essuman · T. Norby
Department of Chemistry, University of Oslo, FERMiO, Gaustadalleen 21, 0349 Oslo, Norway

G. H. Meier
University of Pittsburgh, Pittsburgh, PA, USA

number of recent studies [11–13] have shown that the chromia growth mechanisms in H_2O/H_2 mixtures are substantially different from those in O_2-based gases.

In the present study, the oxidation behaviour of a NiCr-base ODS alloy has been investigated during isothermal oxidation in Ar–20%O_2, Ar–7%H_2O and Ar–4%H_2–7%H_2O at 1000 °C and 1050 °C. Main emphasis was given to the effect of gas composition on the oxide scale growth mechanisms and morphology.

Experimental

The NiCr-based ODS alloy studied was received in the form of a hot forged bar. Table 1 gives the chemical composition determined by Inductively Coupled Plasma Mass Spectrometry (ICPMS) of the ODS alloy and a conventional wrought Ni–25Cr alloy (in weight percent). As frequently described for this type of materials (see e.g. [14]) the microstructure consisted of a mixture of elongated and equiaxed grains. They typically had a size of approximately 100 μm. Specimens of 10 × 10 × 2 mm dimensions were machined from the forged bar, ground to a 1200 grit surface finish using SiC paper and ultrasonically cleaned in acetone immediately before use. Specimens of each alloy were oxidized in three different oxidizing gases, i.e. Ar–20%O_2, Ar–7%H_2O and Ar–4%H_2–7%H_2O. The water vapour content of the reaction gases was adjusted by bubbling Ar or Ar–4%H_2 mixtures of ultra-high purity through deionized water at controlled temperatures.

Isothermal oxidation tests at 1000 °C and 1050 °C were carried out in a Setaram Thermobalance (TG92) for up to 72 h. Individual specimens were suspended on an alumina hook and gravimetric data were recorded continuously during each experiment. The total gas flow rate in the alumina furnace tube was 2 L/h, corresponding to a linear gas velocity of 0.2 cm/s, at a total pressure of 1 bar. The heating rate was 90 °C/min.

In addition to the TG studies, a number of isothermal furnace exposures were carried out in which four specimens were exposed for 5, 8, 25 and 50 h, respectively, in Ar–20%O_2 at 1000 °C. Two other specimens were also exposed for a longer time, i.e. 1000 h in Ar–20%O_2 and Ar–2%H_2O at 1000 °C.

The oxidized specimens were nickel coated, mounted in a resin and subsequently prepared using the conventional metallographic route of grinding, polishing and fine polishing. The metallographic cross sections were analysed by optical metallography and scanning electron microscopy (SEM) with energy dispersive X-ray analysis (EDX).

Results

Figure 1 shows the weight change data during isothermal oxidation of the studied ODS alloy at 1050 °C in the three test gases. Apart from the very early stages of oxidation, the oxidation rates of the (ODS) alloy in the two water vapour containing, low-pO_2 gases are substantially higher than in Ar–O_2. The differences in weight change after 72 h of oxidation are confirmed by the SEM cross sections in Fig. 2, i.e. the scale formed in the low-pO_2 gases are thicker than those formed in Ar–O_2. It is important to notice that the scales are quite non-uniform in thickness. Especially the specimen exposed in Ar–O_2 shows "flat areas" in which the oxide scale is quite thin, whereas in other areas rapidly growing, nodular type oxide growth is found locally. In these areas of nodular growth, the oxide formed in Ar–O_2 tends to be heavily voided and metal seems to be protruded outward from the alloy into the scale. This behaviour is also found after exposure in the wet gases; however, the number of nodules seems to be slightly larger. Also, the presence of voids in the oxide nodules seems to be far less pronounced in the oxide formed in Ar–H_2O and especially in Ar–H_2–H_2O.

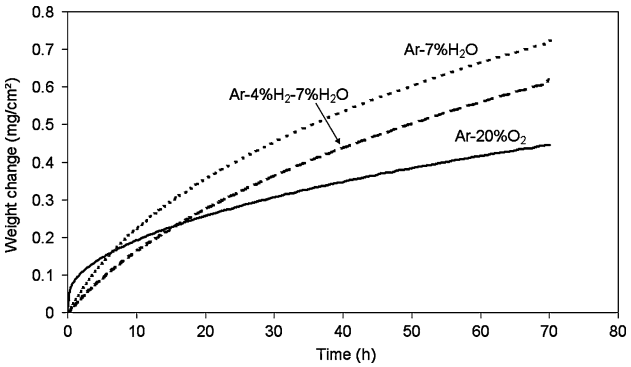

Fig. 1 Weight change versus time during oxidation of the NiCr-base ODS alloy at 1050 °C in different atmospheres

Table 1 Chemical composition of the tested NiCr-base ODS alloy and the conventional wrought Ni–25Cr alloy

Alloy	Composition (wt%)									
	Ni	Cr	N	C	O	Al	Ti	P	S	Y
ODS alloy	Bal.	19.4	0.1156	0.071	0.344	0.2	0.4	<0.01	0.002	0.42
Ni–25Cr	Bal.	24.8	0.0005	0.01	0.0056	–	–	0.01	0.001	–

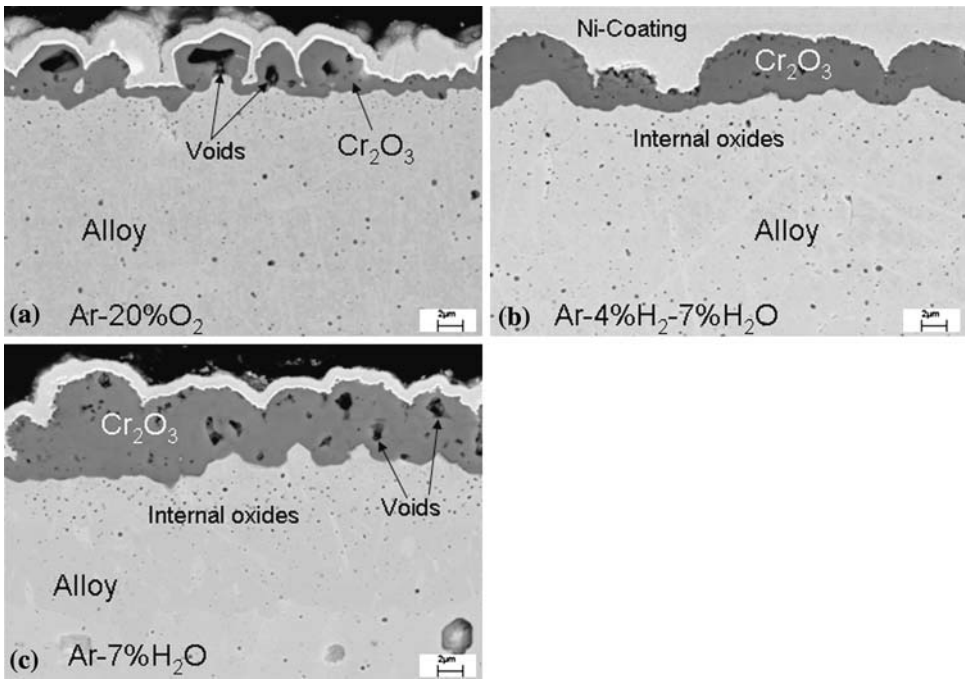

Fig. 2 Cross-section SEM micrographs of NiCr-base ODS alloy after isothermal oxidation for 72 h at 1050 °C in various atmospheres; (**a**) Ar–20%O_2, (**b**) Ar–4%H_2–7%H_2O, (**c**) Ar–7%H_2O. The internal oxide precipitates mainly consist of Al_2O_3

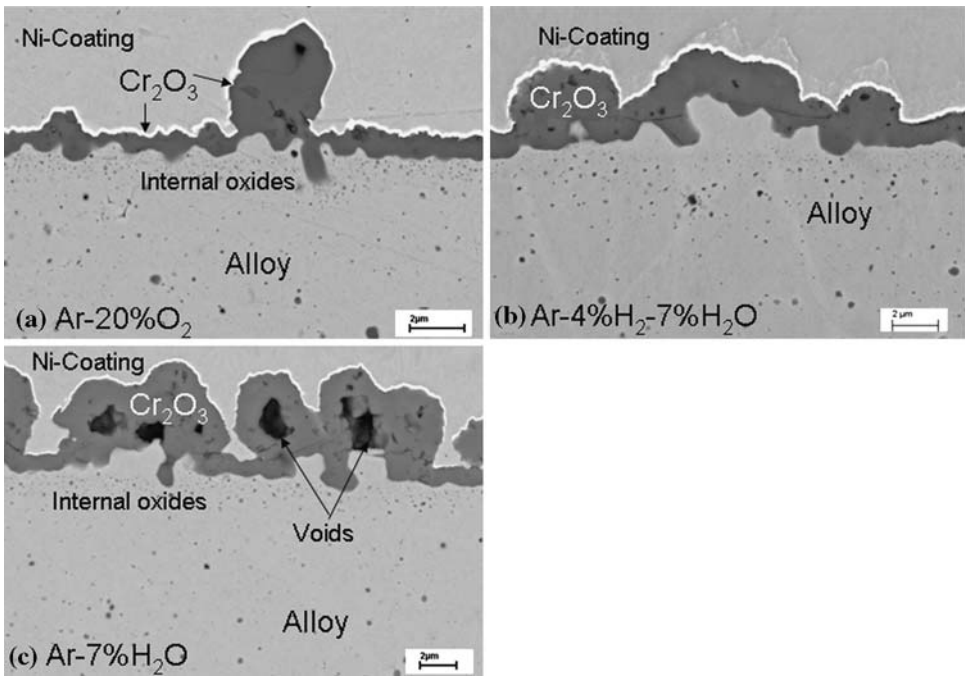

Fig. 3 Cross-section SEM micrographs of NiCr-base ODS alloy after isothermal oxidation for 72 h at 1000 °C in various atmospheres; (**a**) Ar–20%O_2, (**b**) Ar–4%H_2–7%H_2O, (**c**) Ar–7%H_2O. The internal oxide precipitates mainly consist of Al_2O_3

Very similar scale morphologies are found after exposure at 1000 °C (Fig. 3) whereby the number of nodules is smaller than that found at 1050 °C after the same exposure time.

Figure 4 compares the weight changes after 72 h isothermal exposure of the ODS alloy in the various gases with those obtained for the yttria-free, conventional chromia-forming wrought alloy Ni–25Cr. In all cases, the oxide scales on the Y_2O_3-containing alloy are, as expected from literature [7], thinner than those on Ni–25Cr. In spite of these differences in oxidation rate, both materials show the same trend when comparing the behaviour in the three gases, that is, the scales formed in the low-pO_2 gases are thicker than those formed in Ar–O_2, in agreement with findings from various authors for pure chromium and other chromia forming materials [11–13].

Figure 5 shows the time dependence of scale formation in Ar–20%O_2 at 1000 °C. The number of nodules increases with increasing exposure time. After very long term exposure the nodules tend to grow together, thus giving the

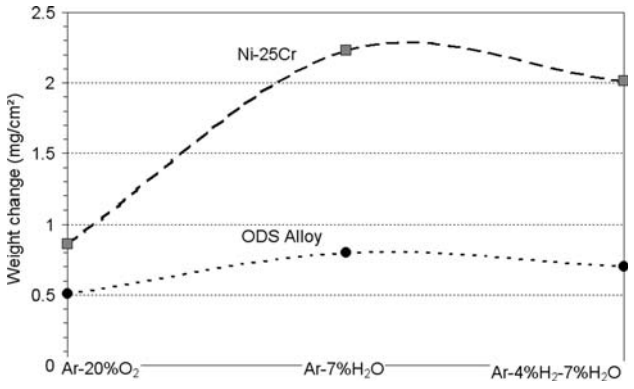

Fig. 4 Weight change after isothermal oxidation of NiCr-base ODS alloy and Ni–25Cr model alloy in different atmospheres at 1050 °C for 72 h. Inserted lines do not present a real pO_2 dependence of the oxidation rate; they are just inserted for clearer visibility of the data points

impression that the scale eventually becomes relatively uniform in thickness (Fig. 6). The outer parts of this type of scales are prone to crack formation during cooling, which is eventually expected to lead to partial scale spalling (Fig. 6).

The formation and location of the nodules is more or less a statistical process with the result that they are quite evenly distributed over the whole metal surface [15, 16]. This is in agreement with metallic nodule formation as a result of other internal corrosion processes (e.g. carburization, nitridation) in cases where the atmosphere did not exhibit external oxide scale formation [17]. The nodule formation is clearly not correlated with alloy grain boundaries considering a typical distance between the nodules of 4–10 μm, compared to an alloy grain size in the range of 100 μm.

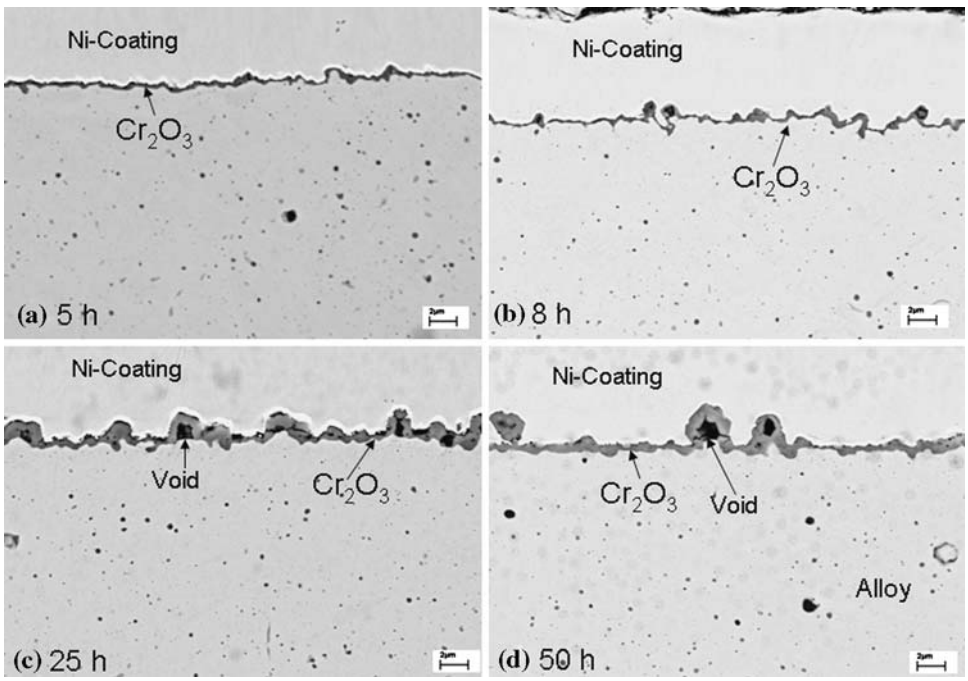

Fig. 5 Cross-section SEM micrographs of NiCr-base ODS alloy after different oxidation times at 1000 °C in Ar–20%O_2

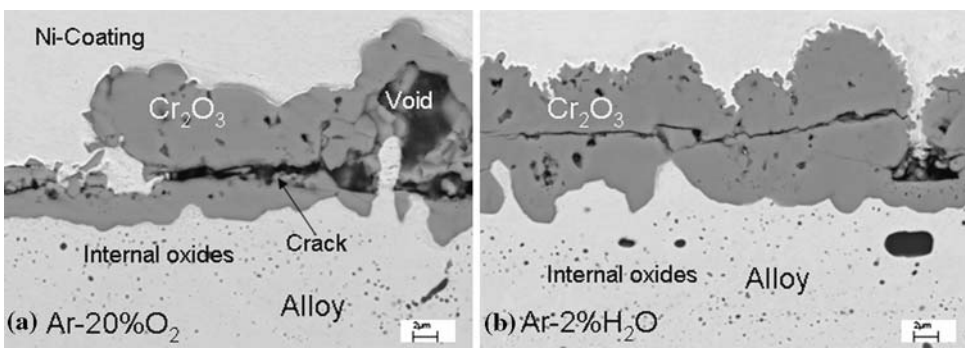

Fig. 6 Cross-section SEM micrographs of NiCr-base ODS alloy after oxidation at 1000 °C in (**a**) Ar–20%O_2 and (**b**) Ar–2%H_2O for 1000 h

Discussion

The non-even oxide growth on an yttria strengthened NiCr-base alloy, whereby "flat" areas with a very thin oxide scale are interspersed with areas of more rapidly growing nodules (Fig. 2a) during air or oxygen exposure, has been described previously (see e.g. [18, 19]). It is well established that the thin oxide grows, due to Y doping, by inward oxygen diffusion, in contrast to chromia scales on non-doped alloys which were shown to mainly grow by outward cation transport [10]. Several mechanisms were proposed to explain the change of the transport process and the decreased growth rate of the chromia scale by a reactive element (RE) addition such as Y. Two popularly supported mechanisms are the grain boundary blocking mechanism in which the RE segregates to oxide grain boundaries [20–22], inhibiting grain boundary diffusion, and the poisoned interface model PIM, in which the reactive elements segregate to the oxide/metal interface, retarding the interface reaction [23–25]. The majority of experiments support the former mechanism, because it was previously clearly demonstrated for various types of chromia forming alloys, e.g. by implanting a RE in a pre-existing oxide scale [26], that the decreased growth rate of chromia scales on RE-doped alloys requires the RE to become incorporated into the oxide scale. When becoming incorporated into the scale, the RE blocks outward cation diffusion [18] resulting in an inwardly growing chromia scale with a lower growth rate than that on non-doped metal or alloy.

Similar findings were recently made for NiO scales on pure Ni [27, 28]. Pre-oxidized Ni samples were coated with CeO_2 and then exposed for an additional 50 h at 800 °C. Cross-sectional micrographs showed that the scale thickness was reduced for the coated nickel with respect to the uncoated nickel. The pre-oxidation treatment did not allow the deposited ceria to contact unoxidized nickel and the reduction of the growth rate of NiO was still observed. These results clearly confirm that the effect of RE oxide on the growth of the oxide scale is not related to the PIM but to the incorporation of the RE in the oxide scale.

If the RE, such as Y, is present as a metallic alloying addition or if it is implanted into the surface [29–31], incorporation into the oxide seems to be a straightforward process because Y might diffuse from the bulk alloy to the scale alloy interface and eventually into the scale. If, however, Y is present in the form of a thermodynamically very stable oxide dispersion, such as in the ODS alloy used in the present study, diffusion of metallic Y is unlikely. For yttria containing Cr-base ODS alloys it was shown that Y incorporation occurs by embedding of the fine yttria dispersion into the inwardly growing oxide scale [32, 33]. An optimum positive effect is thus obtained only if the yttria exists in the alloy in the form of extremely fine dispersions that are practically in direct contact with the scale [32, 33].

From the scale morphology (e.g. Figs. 2, 3) and previous tracer studies [18] it is apparent that in the specimen areas with oxide nodules, the scale grows by outward cation diffusion. Based on the above described theory of the effect of REs on chromia growth, the grain boundary Y doping [34] was apparently not effective in these areas of the scale such that the overall scale growth is substantially higher than would have been obtained in the case of an ideally doped scale. For practical applications it would thus be of great importance to elucidate the reasons for this uneven RE doping.

An important finding in the present study is a small zone of internal oxide precipitates which are formed due to oxidation of the minor alloying addition aluminium (Figs. 2, 3). EDX-analysis revealed the internal oxides to be rich in Al. Due to the small size of the precipitates, unequivocal characterization of the precipitates was not possible by EDX; however, it is believed that the particles consist of alumina, although it cannot be excluded that they consist of an Al-rich, mixed oxide. It has been shown by several authors that the volume increase accompanied by such internal corrosion processes leads to outward metal flow resulting in metallic nodules, which become embedded in the external scale [15, 16], as also found in the present study. Figure 7 clearly shows that in the metallic protrusions, no indication of internal Al-oxide precipitates are found thus strongly indicating that they are formed as a

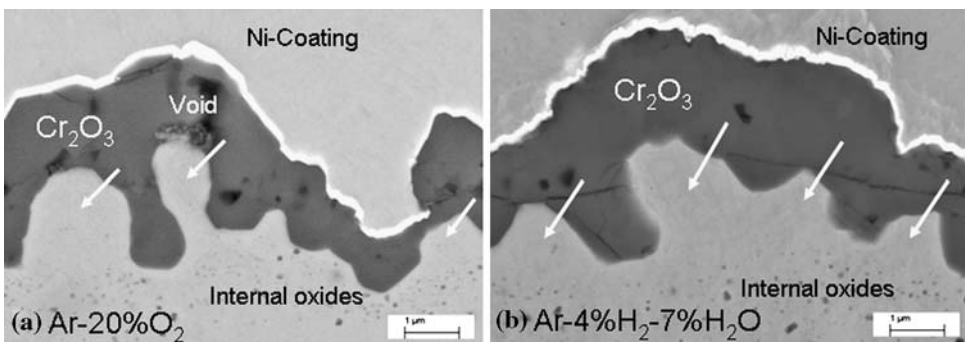

Fig. 7 Cross-section SEM micrographs of NiCr-base ODS alloy after oxidation at 1000 °C in (**a**) Ar–20%O_2 and (**b**) Ar–4%H_2–7%H_2O for 72 h. Arrows indicate metallic protrusions free of internal Al-oxide precipitates

result of the internal oxidation process, thus after the Al in the near-surface zone became depleted.

The outward metal flow must lead to local damage, and thus local loss of protection of the initially formed external surface scale [15, 16]. The question then arises whether the re-healing of the oxide on these metallic protrusions occurs according to the same mechanism as described above for the previously formed, RE-doped thin oxide layer. If only metal flows outward, the metallic nodules will not contain the yttria dispersion present in the bulk alloy. For the reasons mentioned above, the yttria cannot be incorporated into the scale, and the chromia on the metallic nodules will thus grow like that on a non-RE-doped alloy, i.e. by outward cation diffusion. This results in a high growth rate accompanied by substantial void formation due to vacancy condensation near the oxide/alloy interface, as frequently observed for non-RE-doped chromia formers [19]. This explains the typical scale morphology found in the present study after Ar–O_2 exposure (Figs. 2a, 3a).

Several authors illustrated that chromia growth on non-RE-doped alloys in Ar($-H_2$)–H_2O is substantially faster than that in Ar–O_2 or air [11, 12]. It was also found that, the scales are more compact and the void formation at/near the scale/alloy interface is virtually absent resulting in improved oxide adherence. This observation was attributed to the fact that, in addition to outward growth, substantial inward scale growth occurred in the low-pO_2 environment even if no RE doping prevailed [12]. This growth mechanism was attributed to an extremely fine grain size of the oxide scale [12] formed in the low-pO_2 gas.

This at least qualitatively explains the observed scale morphology in the present study after Ar–H_2–H_2O exposure. The thin parts of the scale formed in Ar–H_2–H_2O are slightly thicker than those formed in Ar–O_2 due to differences in grain size and thus number of grain boundaries, which are the transport paths for inwardly diffusing oxygen. Local nodule formation occurs in Ar–H_2–H_2O similar to that in Ar–O_2 because in both cases it is initiated by internal oxidation of Al. The growth of the oxide on the metallic nodules in Ar–H_2–H_2O does, however, not lead to considerable void formation, because substantial inward scale growth occurs [12], in spite of the lack of the Y_2O_3-dispersion in the metallic nodule.

These scale growth mechanisms in the high- and low-pO_2 gases are summarized in Fig. 8. Initially a thin, inwardly growing, Y-doped oxide forms in both environments. The oxide formed in the "flat areas" in Ar–H_2–H_2O is slightly thicker than that formed in Ar–O_2 due to a higher grain boundary density in the oxide formed in the low-pO_2 gas. Local nodular growth occurs in both gases with substantial in-scale voidage during Ar–O_2 exposure. Hardly any voidage occurs in Ar–H_2–H_2O due to a substantial contribution of inward scale growth, in spite of the lack of Y doping.

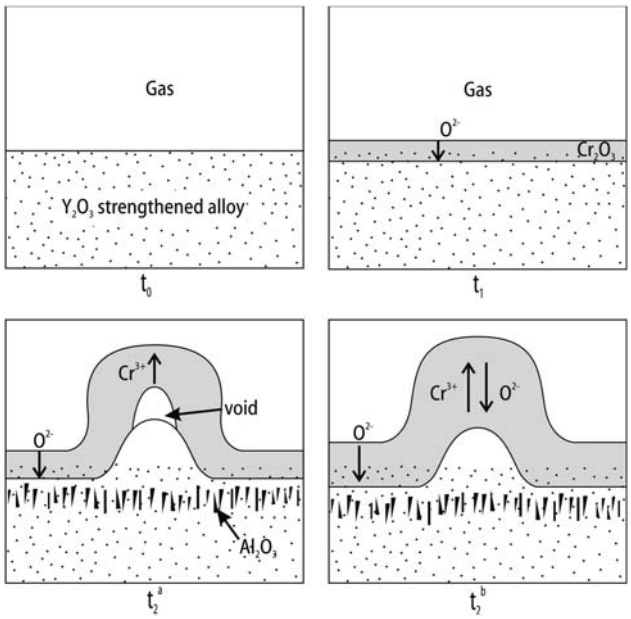

Fig. 8 Schematic diagram showing the mechanism of local "nodule" formation on the ODS alloy during isothermal oxidation at high temperatures. During short-term exposure yttria becomes embedded in the chromia scale (t_1). Y doping results in blocking of outward cation diffusion so that the slowly growing scale grows nearly exclusively via oxygen grain boundary transport. After longer times, internal oxidation of Al results in formation of Y-free metallic protrusions (t_2). Here the oxide grows nearly like that on an yttria-free alloy. Time t_2^a relates to Ar–O_2 exposure, time t_2^b to Ar–H_2–H_2O

The scale found after the Ar–H_2O exposure (Figs. 2c, 3c) seems, in respect to growth rate and morphology, to be intermediate between those formed in the Ar–O_2 and the Ar–H_2–H_2O exposures.

Although the exposure of the metallic inclusions and the respective oxide nodules are found in all atmospheres, their number and size as well as the growth rate of the oxides differ slightly from environment to environment. Based on observations and mechanistic descriptions found in the literature, three reasons which might be responsible for these differences will be discussed:

(1) Enhanced precipitation of internal oxides of Al in the $H_2O(H_2)$ atmosphere compared to Ar–O_2, as recently found for internal Cr-oxide in the case of FeCr alloys [35, 36].
(2) Differences in Ti incorporation into the chromia scale [14] due to a pO_2 dependence of the Ti-solubility in chromia [37].
(3) Dissolved hydrogen or OH^- originating from water vapour altering the defect structure and forming point defects in chromia [38, 39].

To get further insight on the reasons for these differences, a number of specimens were analysed by SNMS after very short exposure times, i.e. when the scales were

still relatively flat and hardly any nodules had formed. The quantification of the SNMS data was carried out using the procedure described in references [40, 41].

A clear indication for mechanism (1) could not be derived from the SEM-cross sections (Figs. 2, 3) and only a minor indication of such an effect might be derived from the SNMS profiles.

Based on the SNMS data in Fig. 9, mechanism (2) might play a role in the development of various morphologies observed in the different environments. A number of studies have shown that Ti-incorporation into the chromia scale results in an increase of the scale growth kinetics probably due to a classical doping mechanism [14, 42]. Naoumidis et al. [37] showed that the Ti solubility in chromia decreases with increasing oxygen partial pressure. During Ar–O_2 exposure substantial Ti solubility will thus only occur in the inner part of the oxide scale. The outward diffusing Ti will in the outer scale hardly be present in the chromia lattice and only prevail as TiO_2 on top of the scale, as confirmed by the SNMS profile in Fig. 9. From the pO_2 dependence of Ti solubility, it is expected that after exposure in the low-pO_2 gas Ti should be more evenly distributed all through the chromia scale, in agreement with the SNMS data in Fig. 9. This higher, overall solubility and a more even distribution of defects may allow more rapid outward Ti cation transport and thus a higher Ti concentration at the scale/gas interface after exposure in low-pO_2 gas compared to high-pO_2 gas (Fig. 9). Enhanced outward chromia scale growth due to Ti doping which was illustrated by several authors [14, 43] is likely to be increased by increased Ti solubility in the scale. This may be an explanation for the differences observed in the different gases.

Another possible explanation would be mechanism (3) where dissolved hydrogen or OH originating from water vapour may form point defects and alter the defect structure of the chromia scale [38, 39]. In stoichiometric oxides protons may be the dominating positive defects even at very low water vapour partial pressures and high temperatures. When protons dominate the defect structure, the defect-related properties, such as transport properties of the oxide, become dependent on the water vapour partial pressure [39]. Hydrogen doping would have the same consequences as Ti doping, namely enhancing the cation outward diffusion. Both form positively charged defects which in turn, to keep the charge balance, promote the additional creation of chromium vacancies.

However, it is not possible to provide experimental evidence for mechanism (3), as in Fig. 9 for (2) the dissolution of Ti in the chromia scale, because hydrogen cannot be quantified using SNMS.

To answer the question whether hydrogen doping plays a role in the present findings additional experimental techniques need to be employed, e.g. gas phase analysis—a technique in which the oxidation process is studied by analysing gas consumption and evolution in a sealed volume by isotope labelling methods during the course of the oxidation reaction or in situ XPS measurements using a synchrotron beam studying adsorption processes and reactions at the oxide scale/gas interface.

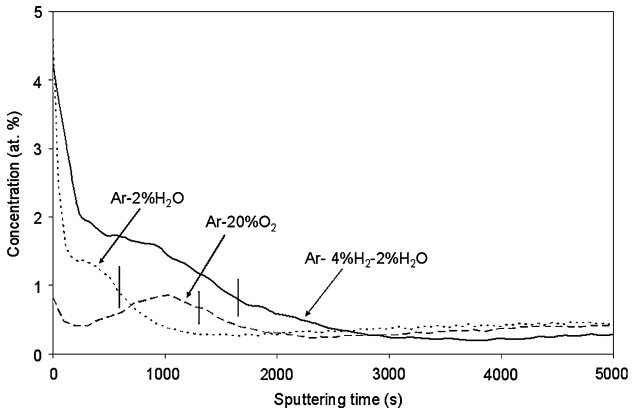

Fig. 9 SNMS profiles for Ti after 2.5 h oxidation of NiCr-base ODS alloy in Ar–20%O_2, Ar–2%H_2O and Ar–4%H_2–2%H_2O, respectively. The lines drawn across the curves for the various environments indicate the respective metal/scale interfaces whereby to the left of these lines is the oxide scale and to the right the alloy

Conclusions

The chromia scale on an yttria dispersion strengthened NiCr-base alloy during Ar–O_2 exposure at 1000 °C and 1050 °C exhibits a very small growth rate. Two types of oxide morphologies are found on the specimen surface:

- "flat areas" with very thin oxide which, based on literature data, grows by inward oxygen diffusion along oxide grain boundaries because of the suppression of the outward chromium transport due to Y doping.
- More rapidly growing oxide nodules which form on metallic protrusions.

The metallic protrusions are the result of internal oxidation, mainly of Al, which leads to a volume increase in the alloy and consequently to local outward metal flow. As the metallic protrusions are free of yttria dispersion, the oxide formed in all test environments on the metallic protrusions exhibits a substantially higher growth rate than in the "flat areas". The scales formed in Ar–H_2–H_2O in the "flat areas" are slightly thicker than those formed in Ar–O_2, in agreement with recent findings for Cr and NiCr alloys. The nodules formed in Ar–O_2 on the metallic protrusions exhibit substantial in-scale voidage. This is not the case in Ar–H_2–H_2O because of a large extent of inward scale growth occurring in this gas even in the absence of

yttrium doping. The growth rate and morphology of the scales formed in the different gases are possibly additionally affected by a pO_2 dependence of Ti solubility in chromia and/or hydrogen doping of the oxide.

Acknowledgements The authors are grateful to Mr. Cosler for carrying out the TG tests and Mr. Wessel for the SEM analyses. The authors are also thankful to the Emmy Noether Program of the German Research Foundation for the financial support.

References

1. Nickel H (1993) Pure Appl Chem 65(12):2481. doi:10.1351/pac199365122481
2. Akhtar A, Hegde S, Reed RC (2006) JOM 58:37. doi:10.1007/s11837-006-0066-0
3. Wallwork GR (1976) Rep Prog Phys 39:401. doi:10.1088/0034-4885/39/5/001
4. Benjamin JS (1970) Metall Trans 1:2943
5. Gilman PS, Benjamin JS (1983) Annu Rev Mater Sci 13:279. doi:10.1146/annurev.ms.13.080183.001431
6. Quadakkers WJ (1990) Werkst Korros 41:659. doi:10.1002/maco.19900411204
7. Hou PY, Stringer J (1995) Mater Sci Eng A 202:1. doi:10.1016/0921-5093(95)09798-8
8. Ramanarayanan TA, Ayer R, Petkovic-Luton R, Leta DP (1988) Oxid Met 29(5/6):445. doi:10.1007/BF00666845
9. Zhang Y, Zhu D, Shores DA (1995) Acta Metall 43(11):4015. doi:10.1016/0956-7151(95)00093-B
10. Przybylski K, Garratt-Reed AJ, Yurek GJ (1988) J Electrochem Soc 135(2):509. doi:10.1149/1.2095646
11. Michalik M, Hänsel M, Zurek J, Singheiser L, Quadakkers WJ (2005) Mater High Temp 22:213
12. Żurek J, Young DJ, Essuman E, Hänsel M, Penkalla HJ, Niewolak L et al (2008) Mater Sci Eng A 477:259. doi:10.1016/j.msea.2007.05.035
13. Galerie A, Wouters Y, Caillet M (2001) Mater Sci Forum 369–372:231
14. Ennis PJ, Quadakkers WJ (1987) In: Marriot JB, Merz M, Nihoul J, Ward JO (eds) High temperature alloys—their exploitable potential, JRC Petten, NL, 15–17th Oct 1985, Elsevier Applied Science London, New York, EUR 11365, p 465
15. Huczkowski P, Ertl S, Piron-Abellan J, Christiansen N, Höfler T, Shemet V et al (2005) Mater High Temp 22:253
16. Hammer JE, Laney SJ, Jackson RW, Coyne K, Pettit FS, Meier GH (2007) Oxid Met 67(1/2):1. doi:10.1007/s11085-006-9041-y
17. Krupp U, Christ H-J (1999) Oxid Met 52(3/4):277. doi:10.1023/A:1018843612011
18. Quadakkers WJ, Holzbrecher H, Briefs KG, Beske H (1989) Oxid Met 32(1/2):67. doi:10.1007/BF00665269
19. Quadakkers WJ, Holzbrecher H, Briefs KG, Beske H (1988) Proceedings of the European Colloquium organized by Commission of the European Communities Directorate General: Science, Research and Development, Petten Establishment, Petten, (N.H.), The Netherlands, p 155
20. Ecer GM, Meier GH (1979) Oxid Met 13(2):159. doi:10.1007/BF00611977
21. Ecer GM, Singh RB, Meier GH (1982) Oxid Met l8:53
22. Haugsrud R, Gunnaes AE, Simon CR (2001) Oxid Met 56(5/6):453. doi:10.1023/A:1012541432639
23. Pieraggi B, Rapp RA (1993) J Electrochem Soc 140(10):2844. doi:10.1149/1.2220920
24. Pieraggi B, Rapp RA, Hirth JP (1995) Oxid Met 44(1/2):63. doi:10.1007/BF01046723
25. Strawbridge A, Rapp RA (1994) J Electrochem Soc 141(7):1905. doi:10.1149/1.2055025
26. Hou P, Brown I, Stringer J (1991) J Nucl Instrum Methods B59(60):1345. doi:10.1016/0168-583X(91)95827-Z
27. Jackson RW, Leonard JP, Pettit FS, Meier GH, Solid State Ionics (in press)
28. Jackson RW, Leonard JP, Niewolak L, Quadakkers WJ, Pettit FS, Meier GH, Mat Sci Forum (in press)
29. Gil A, Mrowec S, Jedliński J (1992) Solid State Ionics 58(1–2):13. doi:10.1016/0167-2738(92)90005-A
30. Hou P, Stringer J (1988) Oxid Met 29(1/2):45
31. Quadakkers WJ, Jedlinski J, Schmidt K, Krasovec M, Borchardt G, Nickel H (1991) Appl Surf Sci 47:261. doi:10.1016/0169-4332(91)90040-Q
32. Quadakkers WJ, Norton JF, Penkalla J, Breuer U, Gil A, Rieck T, Hänsel M (1996) In: Newcomb SB, Little JA (eds) 3rd international conference on microscopy of oxidation, Cambridge, UK, p 221
33. Crone Uvd, Hänsel M, Quadakkers WJ, Vaßen R (1997) Fresenius J Anal Chem 358:230. doi:10.1007/s002160050391
34. Pint BA (2003) Proceedings from the John Stringer symposium on high temperature corrosion, 5–8 Nov 2001, ASM International, Indianapolis, IN, p 9
35. Essuman E, Meier GH, Zurek J, Hänsel M, Quadakkers WJ (2008) Oxid Met 69(3/4):143. doi:10.1007/s11085-007-9090-x
36. Essuman E, Meier GH, Żurek J, Hänsel M, Quadakkers WJ (2007) Scr Mater 57(9):845. doi:10.1016/j.scriptamat.2007.06.058
37. Naoumidis A, Schulze HA, Jungen W, Lersch P (1991) J Eur Ceram Soc 7:55–63. doi:10.1016/0955-2219(91)90054-4
38. Norby T (1986) J Phys 47:849
39. Norby T (1990) Solid State Ionics 41–42:857. doi:10.1016/0167-2738(90)90138-H
40. Quadakkers WJ, Viefhaus H (1995) In: Grabke HJ (ed) Guidelines for methods of testing and research in high temperature corrosion. EFC Publications No. 14, The Institute of Materials, London, p 189
41. Quadakkers WJ, Speier W, Nickel H (1991) Appl Surf Sci 52:271. doi:10.1016/0169-4332(91)90069-V
42. Rabbani R, Ward LP, Strafford KN (2000) Oxid Met 54(1/2):139–153. doi:10.1023/A:1004658814608
43. Nagai H, Okabayashi M (1981) Trans Japan Inst Met 22:691